Talanta 207 (2020) 120257

Contents lists available at ScienceDirect

Talanta

journal homepage: www.elsevier.com/locate/talanta

A DNA electrochemical biosensor based on triplex DNA-templated Ag/Pt nanoclusters for the detection of single-nucleotide variant

Fang Wu[a,1], Qian Lin[b,1], Liangliang Wang[b], Yulian Zou[c], Mei Chen[b], Yaokun Xia[b], Jianming Lan[a], Jinghua Chen[b,*]

[a] Department of Basic Chemistry, School of Pharmacy, Fujian Medical University, Fuzhou, Fujian Province, 350108, China
[b] Department of Pharmaceutical Analysis, School of Pharmacy, Fujian Medical University, Fuzhou, Fujian Province, 350108, China
[c] Institute of Immunotherapy, Fujian Medical University, Fuzhou, Fujian Province, 350108, China

ARTICLE INFO

Keywords:
Triplex DNA-Templated Ag/Pt nanoclusters
Peroxidase-mimic
Single-nucleotide variant
DNA electrochemical biosensor

ABSTRACT

A label-free electrochemical biosensor based on the triplex DNA-templated Ag/Pt bimetallic nanoclusters (triplex-Ag/PtNCs) and locked nucleic acid (LNA) modified X-shaped DNA probe was developed for the detection of single-nucleotide variant (SNV) related to β-thalassemia. Firstly, using triplex DNA as template, a site-specific and homogeneous Ag/PtNCs was prepared, which can effectively catalyze the 3,3,5,5-tetramethylbenzidine-H_2O_2 system and thus be employed as a signal reporter in the field of electrochemical biosensor. Secondly, the LNA modified X-shaped probes were assembled on gold electrode surface, which can only be dissociated in the presence of target, leading to the hybridization with triplex-Ag/PtNCs and significant increase of current signal. In this way, the detection limit for SNV of β-thalassemia was 0.8 fM with variant allele frequency (VAF) as low as 0.0001%.

1. Introduction

As is well known, single-nucleotide variant (SNV) is one of the most significative and common forms of genetic variation [1], and thereby is linked to many diseases such as β-thalassemia (β-Thal) [2], diabetes [3], Alzheimer's disease [4], and cancers [5,6]. Accordingly, SNV becomes one important biomarker for disease diagnostics, drug development, and clinical studies [7,8]. Furthermore, owing to an abundant of wild-type (wt) genes and a low level of variants [9], methods with highly sensitivity and excellent specificity are required toward the accurate and sensitive detection of SNV. Numerous classical approaches [10,11] have been successfully utilized to detect SNV, which are mainly based on allele-specific hybridization methods and incorporated various signaling approaches, including fluorescence [12], solid-state nanopores [13], optical thin-film biosensor chips [14], microfluidic platform [15], electrochemistry [16], and so on. Among these, electrochemistry has gained considerable interest due to its innate features, such as high sensitivity, rapid analysis, easy operation, and low cost [17–19]. However, the classical electrochemical methods were commonly labeled by natural enzymes, such as HRP [19] or small electroactive molecules [20] to generate measurable signal, which will inevitably bring about some complicated or expensive operations and even high background noise or false positive caused by the nonspecific adsorption. Therefore, it is meaningful to develop a label-free, low-cost, simple, and robust electrochemical method or profitable substitution of natural enzymes to better meet the needs of SNV genotyping and early diagnosis of related diseases.

Artificial enzymes, as an alternative to natural enzymes, have been synthesized and applied to biosensor [21–23] for its label-free architecture, high efficiency, excellent stability, and lower cost. Recently, a variety of nanomaterials, such as carbon nanomaterials [24,25], noble-metal nanoparticles [26,27], metal oxide nanomaterials [28], and other composites [29], have also been synthesized as artificial enzymes catalysts (nanozymes) and exhibited conspicuous property of peroxidase-like activity. For example, Zheng et al. [24] developed a graphene dots-based enzyme mimetic with highly-efficient peroxidase-like catalytic activity for biosensing. Dalui et al. [29] structured a colorimetric biosensor based on a novel biomimetic catalyst of CuZnFeS alloy nanocrystals with inherent peroxidase-like activity. Additionally, Cai et al. [30] prepared a bimetallic $Pt_{74}Ag_{26}$ alloy nanoparticles supported on ultrathin MoS_2 nanosheets. Compared to monometallic nanoparticles, $Pt_{74}Ag_{26}$ alloy nanoparticles often displayed enhanced catalytic activity and stability due to its synergistic effect in bimetallic nanoparticles, representing a simple and efficient approach for the synthesis of high-

* Corresponding author.
E-mail address: cjh_huaxue@126.com (J. Chen).
[1] Authors with equal contributions.

https://doi.org/10.1016/j.talanta.2019.120257
Received 16 December 2018; Received in revised form 9 August 2019; Accepted 14 August 2019
Available online 14 August 2019
0039-9140/

quality nanozymes. However, these nanozymes templated by inorganic compounds generally have poor biocompatibility and need extra modifications in the detection of biological molecules. It is worth noting that DNA, a naturally water-soluble, low toxic and biocompatible biomolecule [31], was reported as a favorable platform to construct metal-based nanocomposites for DNA biosensing and other application [32–34] owing to a high affinity of the cytosine base (C-base) for metal cation. Wu et al. [35] deposited DNA-templated silver nanoclusters as electroactive label to measure telomerase activity. This method robustly and reliably amplified the signal and avoided signal-to-noise interferences, displaying an effective approach to enhance the electrochemical signal by DNA-templated metallization. Zheng et al. [36] and Fu et al. [37] also used single-stranded DNA template to synthesize Ag/Pt bimetallic nanoclusters, which likewise showed the advantages of the DNA-templated nanomaterials such as facile synthesis, excellent biocompatibility and peroxidase-like activity. Obviously, the microenvironment of DNA template is vital important to the accurate organization of metallic nanoparticles into sophisticated nanostructures, and so has great effects on the stabilities and mimicking activity of these nanoclusters. Meaningfully, Feng et al. [38] demonstrated a new strategy to create a monometal-based nanocluster (AgNCs) in the predefined position of CG.C$^+$ base site by employing triplex DNA as template. The AgNCs showed excellent homogeneity, site-specific nucleation and growth, and stability against salt, thus was potential to be applied to nanomechanical, DNA origami and electronic applications.

Inspired by the above works, herein, a kind of Ag/Pt bimetallic nanoclusters (to be termed triplex-Ag/PtNCs), was prepared by using a triplex DNA template. As expected, the as-prepared triplex-Ag/PtNCs exhibits advantages of homogeneity and excellent peroxidase-like activity. Then, a label-free electrochemical biosensor based on this triplex-Ag/PtNCs and locked nucleic acid (LNA) modified X-shaped DNA probe proposed by our group [39] was engineered for the direct SNV detection of β-Thal. This kind of X-shaped DNA probe or its analogues, which were designed and optimized properly for targeting SNV sequences in the last few years, revealed high specificity and universality [40–44]. Consequently, with the aid of signal enhancement of triplex-Ag/PtNCs, specific recognition of the LNA modified X-shaped DNA probe, and the merits of electrochemical biosensor, a desired detection limit of 0.8 fM and a variant allele frequency (VAF) of 0.0001% for β-Thal SNV assay were obtained.

2. Experimental

2.1. Materials

All oligonucleotides were synthesized by Sangong Biotech Co., Ltd (Shanghai, China) and their base sequences were illustrated in Table S1 (see details in the Supplementary Information). The concentrations were quantified by A260 based on their individual absorption coefficients, and all of them were HPLC purified. Silver nitrate ($AgNO_3$), sodium borohydride ($NaBH_4$), 3,3,5,5-tetramethylbenzidine (TMB), methylene blue (MB), H_2O_2 and trisodium citrate were purchased from Sinopharm Chemical Reagent Company (Shanghai, China). Dipotassium tetrachloroplatinate (K_2PtCl_4) was purchased from Adamas Reagent Co. Ltd. (Damas-beta). Tris-(hydroxymethyl)-aminomethane (Tris) was purchased from Cxbio Biotechnology Co. Ltd. (Denmark). 6-Mercapto-1-hexano (MCH, 97%), hexaammineruthenium (III) chloride (RuHex, 98%) were purchased from Sigma-Aldrich (USA). The buffer solutions involved in this work were as follows: sodium citrate buffer (10 mM, pH 7.0), DNA immobilization buffer (I-buffer, 10 mM Tris + 1.0 mM EDTA + 0.5 M NaCl, pH 8.0). DNA hybridization buffer (H-buffer, 10 mM Tris + 1.0 mM EDTA + 0.5 M NaCl + 1.0 mM $MgCl_2$, pH 7.0), MCH solution (2 mM MCH in water). All other chemicals were of analytical grade and all solutions were prepared with MilliQ water (18 MΩ · cm).

2.2. Instruments

UV melting curves were measured using a Hitachi Model 2450 UV/Vis Spectrophotometer (Hitachi, Japan). Fluorescence spectra were carried out on a Cary Eclipse Fluorometer (Agilent, USA). The TEM images of the triplex-Ag/PtNCs were acquired on a JEM-1200EX transmission electron microscope (TEM, JEOL, Japan). All electrochemical measurements were carried out in an IGS2000 electrochemical workstation (Guangzhou Ingsens Equipment, China). The electrochemical system is consisted of a gold working electrode (GE, 2 mm in diameter), an auxiliary platinum wire electrode, and an Ag/AgCl reference electrode. A glass cell with flat bottom was used as detection cell.

2.3. Synthesis and characterization of triplex-Ag/PtNCs

Triplex-Ag/PtNCs were prepared by $NaBH_4$ reduction of $AgNO_3$ and K_2PtCl_4 in aqueous solution. In brief, equimolar amounts of template sequences (T1-b, T2-b and T3-b, see details in Table S1), $AgNO_3$ solution and K_2PtCl_4 solution were mixed together in sodium citrate buffer. After incubation in the dark for 10 min, a freshly prepared $NaBH_4$ was added and the mixture was allowed to react for 5 min at 45 °C. Then, the product, i.e., triplex-Ag/PtNCs solution, was slowly cooled to ambient temperature and stored in the dark at 4 °C for further use. Centrifugal operation (13,500 × *g*, 15 min) was carried out before use and the supernatant was carefully collected. Herein, final concentrations were 5 μM for each triplex DNA template, 50 μM for $AgNO_3$, 300 μM for K_2PtCl_4 and 100 μM for $NaBH_4$. UV melting curve of DNA, fluorescence spectra, and TEM were measured for the study of formation and characteristic of the as-prepared triplex-Ag/PtNCs. Triplex-AgNCs used as the control group were also prepared with an identical preparation procedure but without the addition of K_2PtCl_4.

2.4. Enzyme-mimic catalytic activity evaluation of triplex-Ag/PtNCs

The catalytic activity was evaluated on the basis of a catalytic oxidation reaction of the TMB by H_2O_2 according to the literature [37]. That is to say, 10 μL of dispersion solution of triplex-Ag/PtNCs and 20 μL of 500 mM H_2O_2 were added into 130 μL of 200 mM acetate buffer (pH 4.0), and then 40 μL of freshly prepared TMB solutions with different concentrations were added. After reacting for 3 min, the mixtures were scanned by UV/Vis spectrophotometer and the obtained absorption curve indicated the catalytic activity of triplex-Ag/PtNCs. The catalytic activity of triplex-AgNCs was compared under same condition. Additionally, kinetic parameters of triplex-Ag/PtNCs were determined on the basis of Michaelis-Menten equation and Lineweaver-Burk plot.

2.5. Assembly of electrochemical biosensor and electrochemical measurement

The GE was firstly polished with 0.3 and 0.05 μM Al_2O_3 suspension, followed by ultrasonic cleaning in ethanol and water for 5 min, respectively. Then it was electrochemically treated in fresh 0.5 M H_2SO_4 solution between −0.8 and + 1.5 V by cycling the potential until a reproducible CV curve was observed. Finally, GE was rinsed with water and blow-dried with nitrogen, waiting for the following assembly of X-shaped probe. It is generally known that the reproducible formation of high-quality self-assembled monolayer on gold depend largely on the state of electrode surface. Electrochemical oxidation-reduction pretreatment in 0.5 M H_2SO_4 is a commonly used method to regenerate the electrode surfaces, by removing any remaining impurities and producing a reproducible electrode surface with relatively low roughness [45–47].

Afterwards, the pretreated GE was incubated in 2.5 μL of I-buffer containing 0.3 μM thiolated Strand 1 (S1) for 1 h, subsequently in the

MCH solution for 40 min to remove the adsorbed nonspecific oligonucleotides on the GE surface. Then, 2.5 μL of different H-buffer solutions, containing respectively Strand 2 (S2), Strand 3 (S3), and Strand 4 (S4), were successively added to the GE surface and incubated for 1 h. The concentrations for S2, S3, and S4 were 1 μM, 0.4 μM, and 0.6 μM, respectively. After this, 2.5 μL of H-buffer solution containing target DNA, was added to the GE surface and incubated for 1 h. Finally, 4 μL of 5 μM triplex-Ag/PtNCs was added to the GE surface and incubated for 1 h. Unless otherwise noted, washing and drying must be performed following each assembly steps and the incubation was achieved at room temperature.

Electrochemical impedance spectroscopy (EIS) and cyclic voltammetry (CV) were used to monitor each assembly step of GE. EIS was carried out in 0.1 M KCl, 10 mM Tris-HCl and 10 mM $[Fe(CN)_6]^{3-/4-}$ solution (pH 7.0) at a potential of 0.2 V in the frequency range of 0.1–10^5 Hz. A Nyquist plot (Z′ vs -Z″) was drawn to analyze the impedance results. CV was measured in 10 mM Tris-HCl containing 30 μM RuHeX at a scan rate of 500 mV/s with the potential ranging between –0.5 and 0.1 V. SWV was applied to achieve electrochemical signal in 10 mM H_2O_2 before enrichment in 0.2 mM MB, and potential was scanned from −0.6 to 0 V with the following parameters: frequency of 30 Hz, pulse size of 25 mV, and step size of 4 mV.

3. Results and discussion

3.1. Sensing principle of the electrochemical biosensor

The detailed principle of the assay strategy is illustrated in Fig. 1. In this strategy, the as-prepared triplex-Ag/PtNCs was used as a signal reporter for its enzyme-like activity, which would effectively catalyze the hydrogen peroxide-mediated oxidation of MB, along with an emerging electrochemical signal. As shown in Fig. 1A, the triplex-Ag/PtNCs were synthesized by using DNA triplex as a template. In the case of $NaBH_4$ reduction, Ag (I) ion could specifically displace an N3 proton of a cytosine in the $CG.C^+$ base site of triplex DNA to form a new triplet ($CG.CAg^+$), which would stabilize the structure of triplex DNA [38]. Then Pt(0) growth would be triggered on the surface of AgNCs by the galvanic replacement reaction between Pt(II) and Ag(0), and continue by the in-situ reduction with $NaBH_4$ [36]. In particular, one of the single strands in the DNA triplex was much longer than others, which would then hybridize with the proposed LNA modified X-shaped probe. As shown in Fig. 1B, the X-shaped probe compromises four single-stranded DNA. Among these strands, S1 was covalently attached on GE surface through S–Au bonding and partially complementary to the triplex-Ag/PtNCs (colored blue). And S4, containing a LNA modified toehold domain, was partially complementary to the mut DNA (i.e. target SNV of β-thal). In the presence of target, a toehold-mediated strand displacement reaction (TMSDR) was initiated through the hybridization between the target and the external LNA modified toehold of S4, resulting in the dissociation of X-shaped probe into two parts, complex 1 and complex 2, accompanying with the exposure of S1. The complex 2, retaining on the surface of GE, would then hybridize partially with the triplex-Ag/PtNCs, leading to the significant increase of current signal due to high catalytic activity of the triplex-Ag/PtNCs. However, in the absence of the target, this X-shaped probe was stable and thus triplex-Ag/PtNCs cannot hybridize with S1, resulting in hardly any current signal.

3.2. Characterization of triplex-nanoclusters

The fluorescence properties for the triplex-Ag/PtNCs and triplex-AgNCs were compared. As shown in Fig. 2A, obvious fluorescence can be observed from triplex-AgNCs. Moreover, fluorescent emission peaks of the triplex-AgNCs sample were identical to each other over a range of excitation wavelengths, which was unlike the red-shift of other DNA-templated AgNCs systems, demonstrating the homogeneity or there might be just one single species of AgNCs in the triplex-AgNCs. Comparing with the triplex-AgNCs, a nearly complete fluorescence quenching was observed for the triplex-Ag/PtNCs (Fig. S1, Supplementary Information). These results suggested that PtNCs were deposited uniformly on the AgNCs surface, and eventually resulted in the fluorescence quenching of AgNCs [36]. TEM images (Fig. 2B) also showed further evidence that the as-synthesized triplex-Ag/PtNCs were well dispersed and roughly spherical, and the size distribution was about 2 nm in average. The homogeneous nanostructure of triplex-Ag/PtNCs was benefited from the DNA triplet, which can provide site-specific nucleation and in-stiu growth for Ag/PtNCs, as well as considerably decreased the danger of tangling for its much more rigid structure than the two-strand or single-strand.

Melting temperature (T_m) is a useful physical property of nucleic acids and gives information about the stability of DNA structure in a specified environment, so the UV melting curves for both triplex-Ag/PtNCs and triplex DNA without deposited Ag/PtNCs were measured, respectively (Fig. 2A inset). It can be seen that there were two typical melting transitions for both triplex-Ag/PtNCs and triplex DNA, which respectively corresponded to the melting of triplex strands into a single strand and a duplex, and then the duplex into two single strands. These results indicated the formation of triplex DNA or triplex DNA retained its integrity during the synthesis of Ag/PtNCs. Moreover, it was also found that the melting temperature increased in the presence of Ag/PtNCs, validating the Ag/PtNCs could effectively stabilize the structure of triplex DNA.

3.3. Catalytic activity analysis of the triplex-Ag/PtNCs

It has been demonstrated in previous work that DNA-templated Ag/PtNCs have intrinsic peroxidase-like activity. As expected, a strong characteristic emission at 652 nm and 370 nm was observed for triplex-Ag/PtNCs in the TMB-H_2O_2 system, accompanying with the color change of solution (Fig. 3). In contrast, for the triplex-AgNCs prepared under the same condition but without the addition of K_2PtCl_4, no characteristic emission or color variation was observed, representing the deficiency of catalytic activity for triplex-AgNCs. The peroxidase-like activity of triplex-Ag/PtNCs was mainly attributed to the deposition of Pt onto AgNCs, and possible catalytic mechanism of the PtNCs toward TMB/H_2O_2 was considered to be similar with conventional HRP. In brief, H_2O_2 molecules were initially adsorbed on the surface of PtNCs, and were activated to generate hydroxyl radicals (•OH). The resulting •OH which could be stabilized on the surface of the PtNCs, would react with TMB to form a blue color product [48].

To further evaluate the catalytic activity of triplex-Ag/PtNCs, the influence of substrate concentrations upon reaction rates was also studied using the dynamic method. The results showed that the relationship between TMB concentrations and reaction rates followed Michaelis-Menten model (Fig. S2A). In addition, a good linear correlation ($1/v$ = (150.869 ± 4.4073)/[TMB] + (1.524 ± 0.03762), R^2 = 0.9958) for Lineweaver-Burk plot (Fig. S2B) could be obtained, which further indicated that the peroxidation of TMB catalyzed by triplex-Ag/PtNCs was consistent with Michaelis-Menten kinetics. The K_m and V_{max} of triplex-Ag/PtNCs obtained by using Lineweaver-Burk double reciprocal plot were 120.9 μM and 0.312 μM s^{-1}, respectively. Some kinetic parameters of HRP and other metal-based peroxide mimics were also listed in Table S2. K_m value of triplex-Ag/PtNCs was smaller than HRP signifying high affinity of the as-prepared nanozyme for its substrate that helped in achieving a higher V_{max}. The high catalytic activity of Ag/PtNCs was mostly attributed to their homogeneous and small size, as well as synergistic effect among Ag and Pt. The triplex-Ag/PtNCs also displayed smaller or similar K_m as well as higher or similar V_{max} compared with some other metal-based peroxide mimics, suggesting it could act as a promising artificial nanozyme for the design of various electrochemical biosensors on account of its low cost, easy labeling and high stability.

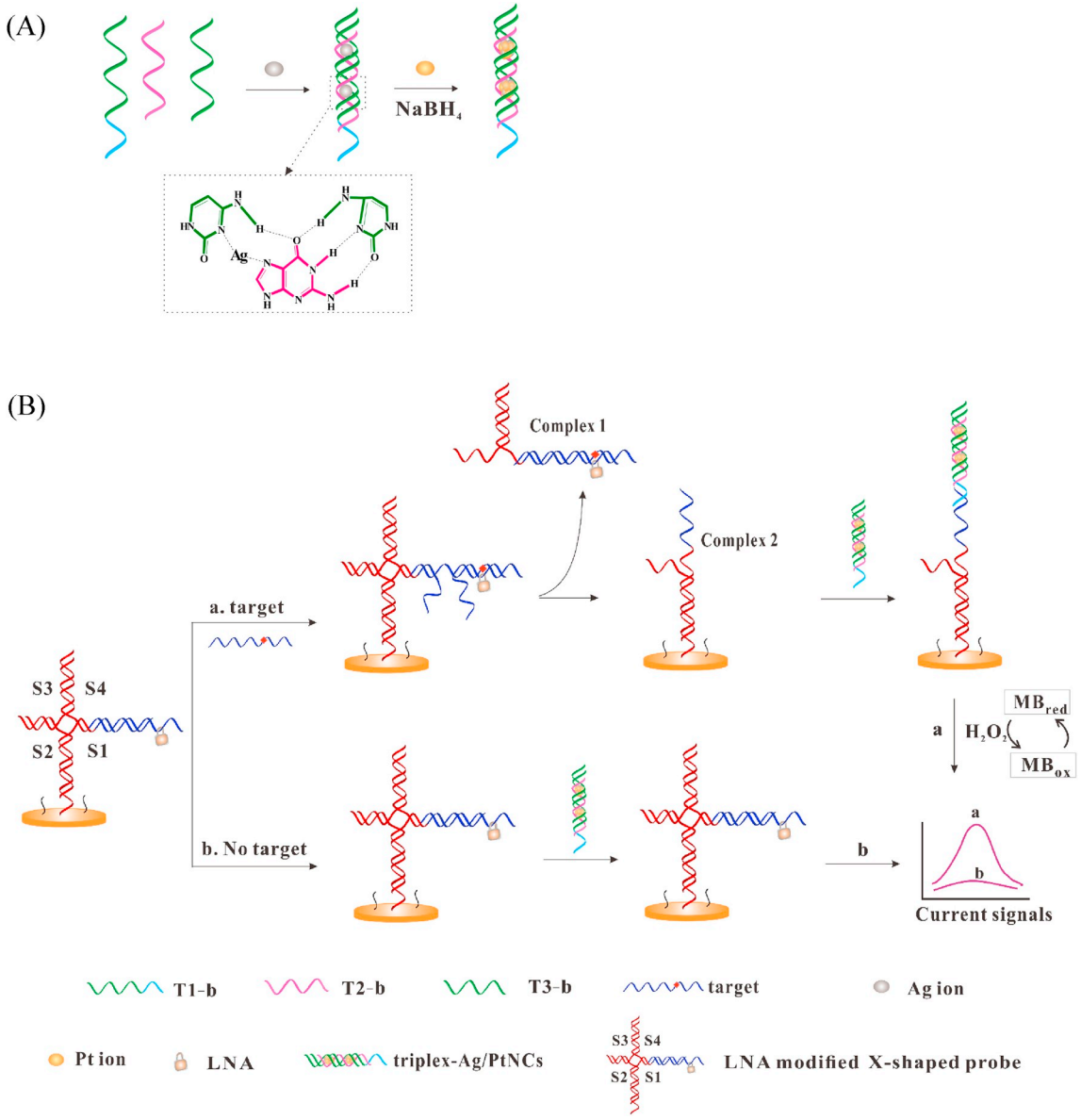

Fig. 1. Schematic illustration of (A) triplex-Ag/PtNCs synthesis protocol, and (B) electrochemical detection of SNV based on the triplex-Ag/PtNCs and LNA modified X-shaped DNA probe.

3.4. Electrochemical characterization of the sensor

In order to confirm X-shaped probe assembly process, EIS for bare GE and different assembly stages of GE were firstly measured. As seen in Fig. 4, the modified GEs showed growing eT resistance (*Ret*) after more and more DNA strands were assembled on the surface of GE. This was due to the fact that more DNA strands resulted in a much denser negative charges on the GE surface, and so generated a much stronger electrostatic repulsion between GE surface and $[Fe(CN)_6]^{3-/4-}$. The results of CVs (showed in Fig. S3) were consistent with that of EIS, suggesting that the X-shaped probe indeed assembled as expected. It also could be found that the eT resistance decreased by the addition of target SNV (Curve e, Fig. 4), which was caused by the TMSDR and the consequent dissociation of some X-shaped probes. Furthermore, SWV was also implemented for different modified electrode to validate the feasibility of our strategy, As shown in Fig. 4 inset, the remarkable current value was only observed for the target + triplex-Ag/PtNCs + X-shaped probe modified GE, yet only very slightly current signals were observed for both triplex-Ag/PtNCs + X-shaped probe modified GE and X-shaped probe modified GE. The results also verified the principle that TMSDR can only be achieved by the addition of target, which brought about the dissociation of X-shaped probe and linking of triplex-Ag/PtNCs, and finally signal enhancement of sensing platform.

3.5. Sensitivity for SNV detection

In order to gain an insight into the sensitivity of the electrochemical biosensor, the SWV spectra were recorded upon the addition of target mut DNA at varying concentrations under the optimized experimental conditions. As shown in Fig. 5, there was nearly no current signal was observed in the absence of mut DNA, while obvious current signal was observed when the concentration of mut DNA was 1.0 fM, indicating the high signal-to-background of this strategy. It was observed that the current values was linearly related to logarithmic concentration of mut DNA in the wide range from 1.0 fM to10.0 nM (Fig. 5 inset). The fitting equation was $y = (0.985 \pm 0.00927)\ x + (1.1728 \pm 0.04499)$ ($R^2 = 0.9988$), where y was the current value, x was the logarithmic concentration (LogC). The detection limit was calculated to be 0.8 fM

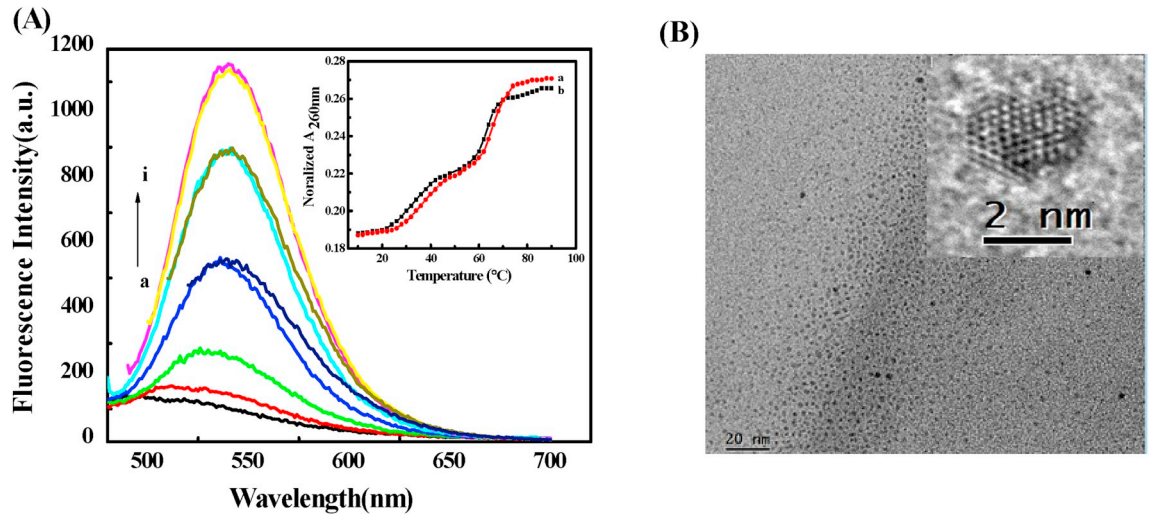

Fig. 2. (A) Fluorescence spectra of triplex-AgNCs obtained at different excitation wavelength (from a to i): 420, 430, 440, 450, 460, 470, 480, 490 and 500 nm respectively. Inset: UV melting curve for triplex-Ag/PtNCs (a), and triplex DNA without deposited Ag/PtNCs (b). (B) TEM images of the triplex-Ag/PtNCs.

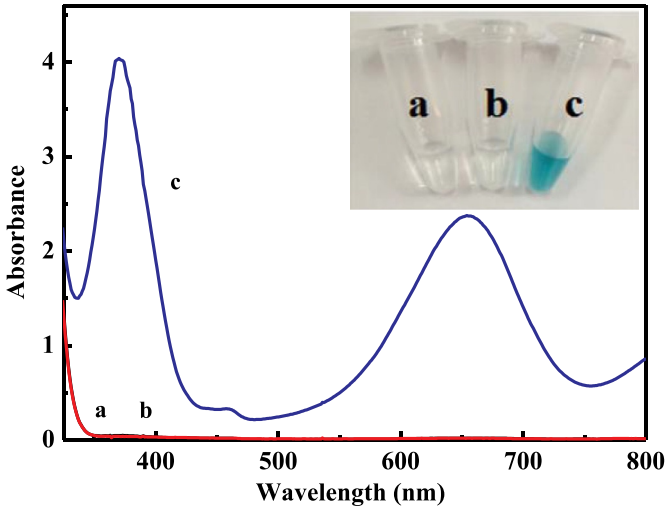

Fig. 3. The UV/vis spectra of blank (a), triplex-AgNCs (b), and triplex-Ag/PtNCs (c). Inset: The color change of TMB-H_2O_2 system for blank (a), triplex-AgNCs (b), and triplex-Ag/PtNCs (c). (For interpretation of the references to color in this figure legend, the reader is referred to the Web version of this article.)

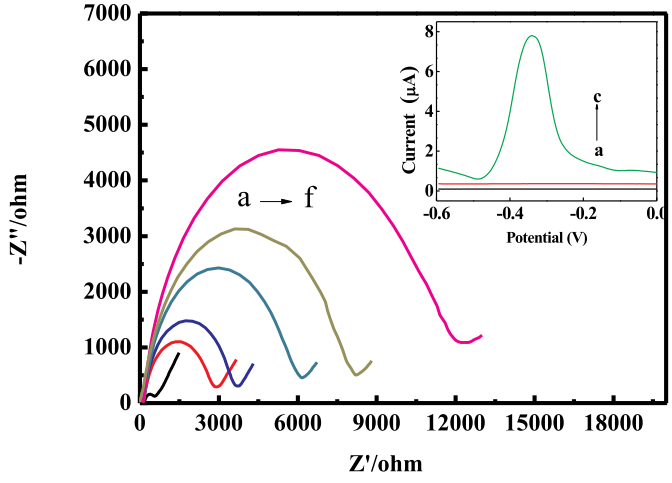

Fig. 4. Nyquist plot of bare GE (a), the S1 modified GE (b), the S1 + S2 modified GE (c), the S1 + S2 + S3 modified GE (d), the target + X-shaped probe modified GE (e), and the S1 + S2 + S3 + S4 modified GE (f). $[Fe(CN)_6]^{3-/4-}$ = 10 mM, [KCl] = 0.1 M. Inset: SWVs obtained from X-shaped probe modified GE (a), triplex-Ag/PtNCs + X-shaped probe modified GE (b), and target + triplex-Ag/PtNCs + X-shaped probe modified GE (c). Frequency 30 Hz, pulse size 25 mV, and step size 4 mV.

when the signal-to-noise ratio was 3. The good sensitivity of this method could be attributed to the introduction of triplex-Ag/PtNCs as a signal amplification resource, which enhanced the current value dramatically due to its steady catalytic activity. The detection range and detection limit comparing with other works were also listed in Table S3. In addition, the relative standard deviation (RSD) of 3 different sensors, which were measured on the same electrode for the detection of 10 pM was 2.4%. And the RSD for three different electrodes was 7.7%, which is agreeable to instrumental analysis.

3.6. Specific discrimination of wt DNA and mut DNA

High specificity is another critical aspect to estimate an analysis method. In order to interrogate the specificity of the proposed method, SWV was also implemented for some control DNA solutions, including mut DNA, wt DNA, random DNA, and no DNA. As shown in Fig. 6, the remarkable current value was only observed for the complete complementary mut DNA, and the almost negligible current values were observed for blank, random DNA, and even for wt DNA with one-base mismatched. The current signal intensity for 10 nM mut DNA was almost 15 times higher than that for wt DNA at the same concentration. It was apparently that the TMSDR was only achieved by using strand exactly matched with mut DNA. To further investigate the ability to discriminate between the mut DNA and the normal wt DNA, some mixed DNA samples, including wt DNA and mut DNA at different molar ratios of 1000,000:1, 100,000:1, 10,000:1, 1000:1, 100:1 and 10:0 (blank) with a total concentration of 10 nM, were prepared and subsequently served as the tested object. From Fig. 6 inset, it can be seen that the current signals dynamically increased with the growing concentration of mut DNA in mixed DNA samples. Even at a concentration ratio as low as 1000,000:1, be equivalent to the 0.0001% variant allele frequency (VAF) of β-Thal, positive control signal can still be identified from the blank by using this sensor. These experimental results indicated a good selectivity of the proposed sensor in the analysis of a rare point mutation even in the presence of a large excess of wide types, which can satisfied well the analysis of real sample. The specificity was benefited from the architecture of X-shaped probe and improved further

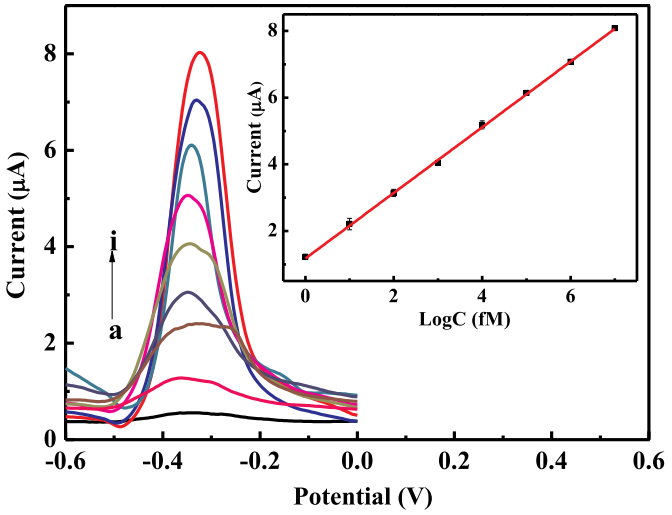

Fig. 5. Sensitivity evaluation of the proposed system. The SWVs for various concentrations of mut DNA (from a to i): 0, 1 fM, 10 fM, 100 fM, 1 pM, 10 pM, 100 pM, 1 nM, and 10 nM, respectively. Frequency 30 Hz, pulse size 25 mV, and step size 4 mV. Inset: the linear relationship between current value and logarithm of mut DNA concentration (Log*C*). Error bars are standard deviations of three repetitive experiments.

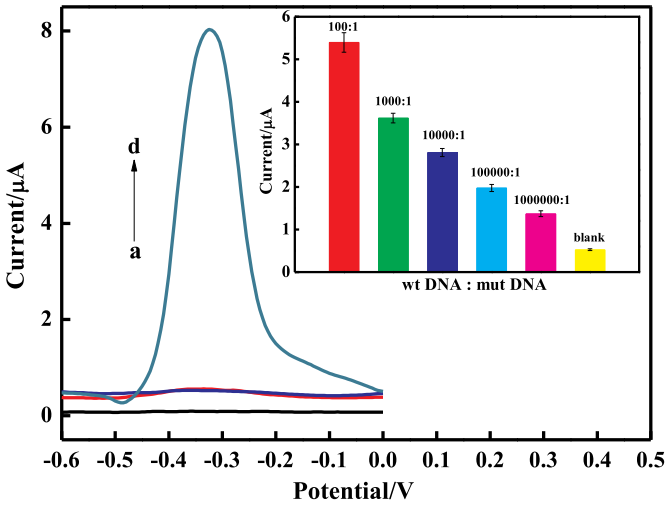

Fig. 6. Specificity investigation. The SWVs of no DNA (a), random DNA (b), wt DNA (c) and mut DNA (d). The concentration of each analyte in the sample is 10 nM; Inset: the SWVs of mixed DNA samples at different molar ratios of wt DNA to mut DNA with a total concentration of 10 nM, error bars represent standard deviations of triplicates. Frequency 30 Hz, pulse size 25 mV, and step size 4 mV.

by LNA integrated into the probe, which had been studied in our previous work [39]. In this work, the LNA modified X-shaped probe was further applied in electrochemical sensors, and its specificity was confirmed again.

4. Conclusion

In summary, a site-specific and homogeneous triplex-Ag/PtNCs was synthesized using triplex DNA as template, and displayed good peroxidase-mimic activity. On this basis, a label-free electrochemical biosensor combining the merits of the triplex-Ag/PtNCs and LNA modified X-shaped DNA probe was developed for the SNV detection of β-Thal, with a detection limit of 0.8 fM and 0.0001% VAF. As far as we know, this was the first attempt to synthesize and apply a triplex DNA-templated Ag/Pt nanoclusters as a signal reporter in the field of electrochemical DNA biosensor, which may represent a promising path toward an attractive signal resource in electrochemical sensor, nanomedicine and other fields. Meanwhile, we also realized that further studies are required to improve its performance. On one hand, the position of the CG.C$^+$ base site in triplex DNA could affect the species of Ag/PtNCs. For example, discrete CG.C$^+$ triplet preferred to form discrete Ag(0) atom rather than AgNCs, which would finally affect the mimic activity of nanoclusters (see Fig. S4). On the other hand, the number of the CG.C$^+$ triplet could also affect the mimic activity (see Fig. S5). Normally, the mimic activity of triplex-Ag/PtNCs should increased with the increasing number of the CG.C$^+$ triplet, but long template length would be unfavorable for the hybridization in electrochemistry because of the steric hindrance. In view of this, triplex-b DNA possessing moderate CG.C$^+$ number and strand length was selected as template in this work. In addition, the strategy might be a potential candidate for the early diagnosis of β-thalassemia or other gene-related diseases due to its sensitivity, specificity, and easy operation.

Acknowledgements

The authors grateful acknowledge the financial support of the National Natural Science Foundation of China (21874019, 21375017), the Natural Science Foundation of Fujian Province, China (2015J01596, 2017J07001), Fujian Science and Technology Innovation Joint Found Project (2016Y9050), the Medical Elite Cultivation Program of Fujian, P.R.C (2014-ZQN-ZD-26), the National Science Foundation for Distinguished Young Scholars of Fujian Province (2013J06003), Program for New Century Excellent Talents of Colleges and Universities in Fujian Province (JA13130).

Appendix A. Supplementary data

Supplementary data to this article can be found online at https://doi.org/10.1016/j.talanta.2019.120257.

References

[1] F.S. Collins, L.D. Brooks, A. Chakravarti, A DNA polymorphism discovery resource for research on human genetic variation, Genome Res. 8 (1998) 1229–1231.
[2] S. Rivella, E. Rachmilewitz, Future alternative therapies for β-thalassemia, Expert Rev. Hematol. 2 (2009) 685–697.
[3] J.P. Lewis, N.D. Palmer, P.J. Hicks, M.M. Sale, C.D. Langefeld, B.I. Freedman, J. Divers, D.W. Bowden, Association analysis in African Americans of European-derived type 2 diabetes single nucleotide polymorphisms from whole-genome association studies, Diabetes 57 (2008) 2220–2225.
[4] Y.C. Chen, C.J. Hsiao, C.C. Jung, H.H. Hu, J.H. Chen, W.C. Lee, J.M. Chiou, T.F. Chen, Y. Sun, L.L. Wen, P.K. Yip, Y.M. Chu, C.J. Chen, H.I. Yang, Performance metrics for selecting single nucleotide polymorphisms in late-onset Alzheimer's disease, Sci. Rep. 6 (2016) 36155.
[5] S.D. Bailey, K. Desai, J.K. Kron, P. Mazrooei, N.A. Sinnott-Armstrong, A.E. Treloar, M. Dowar, K.L. Thu, D.W. Cescon, Noncoding somatic and inherited single-nucleotide variants converge to promote ESR1 expression in breast cancer, Nat. Genet. 48 (2016) 1260–1266.
[6] H. Zafar, Y. Wang, L. Nakhleh, N. Navin, K. Chen, Monovar: single-nucleotide variant detection in single cells, Nat. Methods 13 (2016) 505–507.
[7] D. Wang, W. Tang, X. Wu, X. Wang, G. Chen, Q. Chen, N. Li, F. Liu, Highly selective detection of single-nucleotide polymorphisms using a quartz crystal microbalance biosensor based on the toehold-mediated strand displacement reaction, Anal. Chem. 84 (2012) 7008–7014.
[8] S. Hu, W. Tang, Y. Zhao, N. Li, F. Liu, Ultra-specific discrimination of single-nucleotide mutations using sequestration-assisted molecular beacons, Chem. Sci. 8 (2017) 1021–1026.
[9] Y. Feng, F. Sun, N. Wang, J. Lei, H. Ju, Ru (bpy)$_3^{2+}$ incorporated luminescent polymer dots: double-enhanced electrochemiluminescence for detection of single-nucleotide polymorphism, Anal. Chem. 89 (2017) 7659–7666.
[10] K. Chang, S. Deng, M. Chen, Novel biosensing methodologies for improving the detection of single nucleotide polymorphism, Biosens. Bioelectron. 66 (2015) 297–307.
[11] Q. Xu, S.Q. Huang, F. Ma, B. Tang, C.Y. Zhang, Controllable mismatched ligation for bioluminescence screening of known and unknown mutations, Anal. Chem. 88 (2016) 2431–2439.
[12] Y. Cheng, Q. Du, L. Wang, H. Jia, Z. Li, Fluorescently cationic conjugated polymer as an indicator of ligase chain reaction for sensitive and homogeneous detection of

single nucleotide polymorphism, Anal. Chem. 84 (2012) 3739–3744.
[13] J. Kong, J. Zhu, U.F. Keyser, Single molecule based SNP detection using designed DNA carriers and solid-state nanopores, Chem. Commun. 53 (2017) 436–439.
[14] X. Zhong, R. Reynolds, J.R. Kidd, K.K. Kidd, R. Jenison, R.A. Marlar, D.C. Ward, Single-nucleotide polymorphism genotyping on optical thin-film biosensor chips, Proc. Natl. Acad. Sci. 100 (2003) 11559–11564.
[15] M. Cui, H. Feng, D. Guo, D. Wang, B. Zheng, A droplet-based microfluidic platform for kinetics-based detection of single nucleotide variation at room temperature with large discrimination factors, Sens. Actuators B Chem. 253 (2017) 731–737.
[16] S. Shin, B.Y. Won, C. Jung, S.C. Shin, D.Y. Cho, S.S. Lee, H.G. Park, Electrochemical detection of DNA mutations on a PNA-modified electrode utilizing a single-stranded DNA specific endonuclease, Chem. Commun. 47 (2011) 6611–6613.
[17] Y. Guo, Y. Guo, C. Dong, Ultrasensitive and label-free electrochemical DNA biosensor based on water-soluble electroactive dye azophloxine-functionalized graphene nanosheets, Electrochim. Acta 113 (2013) 69–76.
[18] A.H. Yang, K. Hsieh, A.S. Patterson, B.S. Ferguson, M. Eisenstein, K.W. Plaxco, H.T. Soh, Accurate zygote-specific discrimination of single-nucleotide polymorphisms using microfluidic electrochemical DNA melting curves, Angew. Chem. 53 (2014) 3163–3167.
[19] dÁ.B. Esteban-Fernández, E. Araque, S. Campuzano, M. Pedrero, B. Dalkiran, R. Barderas, R. Villalonga, E. Kiliç, J.M. Pingarrón, Dual functional graphene derivative-based electrochemical platforms for detection of the TP53 gene with single nucleotide polymorphism selectivity in biological samples, Anal. Chem. 87 (2015) 2290–2298.
[20] Y. Huang, Y.L. Zhang, X. Xu, J.H. Jiang, G.L. Shen, R.Q. Yu, Highly specific and sensitive electrochemical genotyping via gap ligation reaction and surface hybridization detection, J. Am. Chem. Soc. 131 (2009) 2478–2480.
[21] H. Wei, E. Wang, Nanomaterials with enzyme-like characteristics (nanozymes): next-generation artificial enzymes, Chem. Soc. Rev. 42 (2013) 6060–6093.
[22] Y. Lin, J. Ren, X. Qu, Catalytically active nanomaterials: a promising candidate for artificial enzymes, Acc. Chem. Res. 47 (2014) 1097–1105.
[23] L. Shabnam, S.N. Faisal, A.K. Roy, I. Minett, V.G. Gomes, Nonenzymatic multispecies sensor based on Cu-Ni nanoparticle dispersion on doped graphene, Electrochim. Acta 224 (2017) 295–305.
[24] A.X. Zheng, Z.X. Cong, J.R. Wang, J. Li, H.H. Yang, G.N. Chen, Highly-efficient peroxidase-like catalytic activity of graphene dots for biosensing, Biosens. Bioelectron. 49 (2013) 519–524.
[25] J. Tian, Q. Liu, A.M. Asiri, A.H. Qusti, A.O. Al-Youbi, X. Sun, Ultrathin graphitic carbon nitride nanosheets: a novel peroxidase mimetic, Fe doping-mediated catalytic performance enhancement and application to rapid, highly sensitive optical detection of glucose, Nanoscale 5 (2013) 11604–11609.
[26] P.C. Pandey, A. Prakash, A.K. Pandey, Studies on electrochemical and peroxidase mimetic behavior of Prussian blue nanoparticles in presence of Pd-WO_3-SiO_2 Nanocomposite; bioelectro-catalytic sensing of H_2O_2, Electrochim. Acta 127 (2014) 132–138.
[27] J. Lan, W. Xu, Q. Wan, X. Zhang, J. Lin, J. Chen, J. Chen, Colorimetric determination of sarcosine in urine samples of prostatic carcinoma by mimic enzyme palladium nanoparticles, Anal. Chim. Acta 825 (2014) 63–68.
[28] Y. Wang, B. Zhou, S. Wu, K. Wang, X. He, Colorimetric detection of hydrogen peroxide and glucose using the magnetic mesoporous silica nanoparticles, Talanta 134 (2015) 712–717.
[29] A. Dalui, B. Pradhan, U. Thupakula, A.H. Khan, G.S. Kumar, T. Ghosh, B. Satpati, S. Acharya, Insight into the mechanism revealing the peroxidase mimetic catalytic activity of quaternary CuZnFeS nanocrystals: colorimetric biosensing of hydrogen peroxide and glucose, Nanoscale 7 (2015) 9062–9074.
[30] S. Cai, Q. Han, C. Qi, Z. Lian, X. Jia, R. Yang, C. Wang, $Pt_{74}Ag_{26}$ nanoparticle-decorated ultrathin MoS_2 nanosheets as novel peroxidase mimics for highly selective colorimetric detection of H_2O_2 and glucose, Nanoscale 8 (2016) 3685–3693.
[31] R. Hu, X. Zhang, Z. Zhao, G. Zhu, T. Chen, T. Fu, W. Tan, DNA nanoflowers for multiplexed cellular imaging and traceable targeted drug delivery, Angew. Chem. 126 (2014) 5931–5936.
[32] J. Tao, P. Zhao, J. Zheng, C. Wu, M. Shi, J. Li, Y. Li, R. Yang, Electrochemical detection of type 2 diabetes mellitus-related SNP via DNA-mediated growth of silver nanoparticles on single walled carbon nanotubes, Chem. Commun. 51 (2015) 15704–15707.
[33] J. Chen, X. Zhang, S. Cai, D. Wu, M. Chen, S. Wang, J. Zhang, A fluorescent aptasensor based on DNA-scaffolded silver-nanocluster for ochratoxin A detection, Biosens. Bioelectron. 57 (2014) 226–231.
[34] T.A.C. Kennedy, J.L. Maclean, J. Liu, Blue emitting gold nanoclusters templated by poly-cytosine DNA at low pH and poly-adenine DNA at neutral pH, Chem. Commun. 48 (2012) 6845–6847.
[35] L. Wu, J. Wang, J. Ren, X. Qu, Ultrasensitive telomerase activity detection in circulating tumor cells based on DNA metallization and sharp solid-state electrochemical techniques, Adv. Funct. Mater. 24 (2014) 2727–2733.
[36] C. Zheng, A.X. Zheng, B. Liu, X.L. Zhang, Y. He, J. Li, H.H. Yang, G. Chen, One-pot synthesized DNA-templated Ag/Pt bimetallic nanoclusters as peroxidase mimics for colorimetric detection of thrombin, Chem. Commun. 50 (2014) 13103–13106.
[37] X.M. Fu, Z.J. Liu, S.X. Cai, Y.P. Zhao, D.Z. Wu, C.Y. Li, J.H. Chen, Electrochemical aptasensor for the detection of vascular endothelial growth factor (VEGF) based on DNA-templated Ag/Pt bimetallic nanoclusters, Chin. Chem. Lett. 27 (2016) 920–926.
[38] L. Feng, Z. Huang, J. Ren, X. Qu, Toward site-specific, homogeneous and highly stable fluorescent silver nanoclusters fabrication on triplex DNA scaffolds, Nucleic Acids Res. 40 (2012) e122.
[39] F. Wu, M. Chen, J. Lan, Y. Xia, M. Liu, W. He, C. Li, X. Chen, J. Chen, A universal locked nucleic acid-integrated X-shaped DNA probe design for amplified fluorescence detection of single-nucleotide variant, Sens. Actuators B Chem. 241 (2017) 123–128.
[40] J.S. Wang, Y.H. Yan, D.Y. Zhang, Modular probes for enriching and detecting complex nucleic acid sequences, Nat. Chem. 9 (2017) 1222–1228.
[41] X. Chen, D. Zhou, H. Shen, H. Chen, W. Feng, G. Xie, A universal probe design for colorimetric detection of single-nucleotide variation with visible readout and high specificity, Sci. Rep. 6 (2016) 20257.
[42] M. Stancescu, T.A. Fedotova, J. Hooyberghs, A. Balaeff, D.M. Kolpashchikov, Non-equilibrium hybridization enables discrimination of a point mutation within 5-40 °C, J. Am. Chem. Soc. 138 (2016) 13465–13468.
[43] J.S. Wang, D.Y. Zhang, Simulation-guided DNA probe design for consistently ultraspecific hybridization, Nat. Chem. 7 (2015) 545–553.
[44] Y.V. Gerasimova, D.M. Kolpashchikov, Detection of bacterial 16S rRNA using a molecular beacon-based X sensor, Biosens. Bioelectron. 41 (2013) 386–390.
[45] J.C. Hoogvliet, M. Dijksma, B. Kamp, W.P. van Bennekom, Electrochemical pretreatment of polycrystalline gold electrodes to produce a peproducible surface roughness for self-assembly: a study in phosphate buffer pH 7.4, Anal. Chem. 72 (2000) 2016–2021.
[46] R.F. Carvalhal, R.S. Freire, L.T. Kubota, Polycrystalline gold electrodes: a comparative study of pretreatment procedures used for cleaning and thiol self-assembly monolayer formation, Electroanalysis 17 (2005) 1251–1259.
[47] J. Zhang, S. Song, L. Wang, D. Pan, C. Fan, A gold nanoparticle-based chronocoulometric DNA sensor for amplified detection of DNA, Nat. Protoc. 2 (2007) 2888–2895.
[48] Z. Gao, M. Xu, L. Hou, G. Chen, D. Tang, Irregular-shaped platinum nanoparticles as peroxidase mimics for highly efficient colorimetric immunoassay, Anal. Chim. Acta 776 (2013) 79–86.